Eur. Phys. J. D **36**, 1–9 (2005)
DOI: 10.1140/epjd/e2005-00181-x

THE EUROPEAN PHYSICAL JOURNAL D

The study of dominant physical processes in the time-resolved optogalvanic spectra of neon

S. Mahmood, M. Anwar-ul-Haq, M. Riaz, and M.A. Baig[a]

Atomic and Molecular Physics Laboratory, Department of Physics, Quaid-i-Azam University, Islamabad 45320, Pakistan

Received 10 November 2004 / Received in final form 10 March 2005
Published online 12 July 2005 –

Abstract. We present the dominant physical processes responsible for the production of the optogalvanic signal in the spectra of neon. We have investigated the effects on the optogalvanic signal by scanning a dye laser across the neon transitions in the DC discharge plasma. Time-resolved spectra are obtained at a fixed wavelength of the dye laser resonantly tuned to an optically allowed transition. The temporal evolutions of the signals are registered on a storage oscilloscope. Three transitions from the $3s[1/2]_2$ metastable state corresponding to the $\Delta J = \Delta K = 0, \pm 1$ dipole selection rules have been selected to investigate the dominant physical processes responsible for the optogalvanic signals. The change in the signal amplitude as a function of the discharge current has been registered. In addition the electron collisional ionization rate parameter ratios have been determined for the transitions corresponding to dipole selection rules $\Delta J = \Delta K = -1$, $\Delta J = \Delta K = 1$ and $\Delta J = \Delta K = 0$, as 1.63, 1.75 and 1.0 respectively. The effective lifetimes of the upper levels involved in the aforementioned transitions are also calculated as 62.5 μs, 31.25 μs and 12.85 μs respectively.

PACS. 32.30.Jc Visible and ultraviolet spectra – 32.80.Rm Multiphoton ionization and excitation to highly excited states (e.g., Rydberg states)

1 Introduction

The optogalvanic effect is a sensitive and convenient method for detecting optical transitions in plasma. The advent of tunable dye lasers has revolutionized the field of laser spectroscopy, in particular the use of the optogalvanic effect for the spectroscopic studies of atoms and molecules. Green et al. [1] pioneered the laser optogalvanic spectroscopy based on irradiation of the discharge with a tunable dye laser. The signal was detected by recording the change in the impedance of the discharge. The optogalvanic effect in the inert gases has been widely studied and different models have been proposed to account for this effect. These models characterize the response of the discharge when the laser is in resonance to a transition and consequently perturbs the steady state population distribution.

Peper et al. [2] developed a theoretical model using the rate equation approach for the analysis of the optogalvanic signal in the case of a three level atom. The rate equations were solved using the modified Schottky-formulation. The effects of radiation trapping, elastic collisions and buffer gas pressure were also discussed. Erez et al. [3] described a phenomenological model of the optogalvanic effect. They defined an electron multiplication factor, which is equal to unity under the steady state condition. This model was successfully used to calculate the relative magnitude, sign and temporal behaviour of various optogalvanic signals. Lawler [4] presented a linear, steady state, analytical model for the optogalvanic effect. The magnitude of the optogalvanic signal from the ionization rate was also predicted. The absolute magnitude of the signal was measured as a function of the positive column radius, the column pressure and the laser intensity. Doughty and Lawler [5] developed a quantitative model, which describes well the optogalvanic signals. This model is an application of linear, steady state perturbation theory to the key rate equations, which describe the discharge. Absolute magnitude of the effect, rate coefficients and absolute densities of the $2p^5 3s$ levels were also determined. Veldhuizen et al. [6] reported a five level model to account the effects of electronic collision and radiative decay in neon discharge plasma. Variation in the population densities of the excited states was also related to the change in the discharge voltage. DeMarinis and Sasso [7] reported a theoretical model for the analysis of the optogalvanic effect, which is based on a balanced equation approach for electron and ion current. In case of small optogalvanic signal the perturbed equations give an analytical expression of the current change in terms of more significant parameter of the discharge. Stewart et al. [8] constructed a rate equation model for the optogalvanic effect in the positive

[a] e-mail: baig@qau.edu.pk

column of the neon glow discharge. This model includes the ground state atom and electron collisional coupling processes. It was demonstrated that the electron transfer plays a dominant role in determining the magnitude and sign of the optogalvanic effect. Han et al. [9] presented a theoretical model, which quantitatively characterizes the dominant physical processes responsible for the optogalvanic signal in the discharge plasma. This model, with only five parameters, reproduced the experimentally obtained time-resolved optogalvanic signals.

In the present work, the experimentally observed time-resolved optogalvanic signals associated with neon transitions $\Delta J = \Delta K = 0, \pm 1$ from the $3s[3/2]_2$ metastable level, have been chosen to investigate the collisional ionization of the excited levels of neon atoms in a gas discharge plasma. The observed signals are fitted to an expression, as presented by Han et al. [9], and extracted the parameters that determine the amplitude and decay rates in the above mentioned transitions. The effect of the current variation on the signal's amplitude is also observed. In addition collisional ionization rate parameters and effective lifetimes of the levels involved in the transitions corresponding to $\Delta J = \Delta K = 0, \pm 1$ have been calculated.

2 Experimental set-up

Our experimental arrangement to study the behavior of optogalvanic signal is similar to that described in our earlier work [10]. A Nd:YAG laser (Spectra Physics, GCR-11) operated at 10 Hz repetition rate and 5 ns pulse duration was used to pump a locally fabricated Hanna type dye laser using a 2400 lines/mm holographic grating. The line width of the dye laser was about ≤ 0.3 cm^{-1}. The dye laser beam to divide it into three parts by inserting beam splitters in the optical path. One portion about 10% of the laser beam was directed through a 1 mm diameter aperture to a neon filled hollow cathode lamp. The second portion about 10% of the beam passed through a 1 mm thick solid etalon (FSR 3.33 cm^{-1}). The third beam was used to trigger the oscilloscope. The hollow cathode lamp was operated through a regulated DC power supply capable of delivering 200 V and 20 mA. The diameter of the cathode was 3 mm, the depth of the hole was 8 mm and the neon gas pressure was 12 torr (Photron, Australia). A 10 kΩ current limiting load resistor was inserted in series with the hollow cathode lamp and the DC power supply. Therefore, an increase in the voltage across the discharge tube upon laser irradiation was accompanied by a corresponding decrease in the discharge current, and vice versa. The laser pulse, tuned in resonance with a certain atomic transition causes a change in the steady-state condition of the discharge. This change was monitored via a coupling capacitor 0.01 μF to a boxcar integrator. By varying the discharge current in a specified range, a set of time-resolved optogalvanic signal was gathered to reveal the effect of the discharge. Time-resolved signals were registered on a storage oscilloscope. The time-integrated signal and the etalon rings were accumulated on a boxcar averager (SRS 250) and an averaged output was stored on a computer for further analysis.

3 Results and discussion

The ground state electronic configuration of neon is $1s^2 2s^2 2p^6\ ^1\mathrm{S}_0$. The excited states follow the intermediate-coupling $j_c K$ coupling scheme $[\{(\ell_1,s_1)j_c,\ \ell_2\}K,s_2]_J$ proposed by Racah [11] and Cowan [12]. In this coupling the orbital angular momentum ℓ_2 of the excited electron couples with the total angular momentum j_c of the core to give the resultant angular momentum K as $[j_c \pm \ell_2]$. The angular momentum K is then weakly coupled with the spin angular momentum s_2 of the excited electron to give the total angular momentum J as $[K \pm s_2]$. The energy levels are denoted as $n\ell[K]_J$. Under this scheme the first excited state for neon $2p^5 3s$ gives rise to four levels namely $3s[3/2]_2$, $3s[3/2]_1$, $3s[1/2']_0$ and $3s[1/2']_1$. Here prime refers to the terms generated from the $2p^5\ ^2\mathrm{P}_{1/2}$ parent ion level. The $3s[3/2]_2$ and $3s[1/2']_0$ levels are metastable, with radiative life times of the order of seconds [13], while the other two levels $2p^5 3s[3/2]_1$ and $2p^5 3s[1/2']_1$ have short radiative life times, 16 ns and 1.2 ns respectively [14]. The second group of excited states arises from the $2p^5 3p$ configuration that reveals ten energy levels designated by $3p[3/2']_2$, $3p[3/2']_1$, $3p[1/2']_1$, $3p[1/2']_0$, $3p[5/2]_3$, $3p[5/2]_2$, $3p[3/2]_2$, $3p[3/2]_1$, $3p[1/2]_1$ and $3p[1/2]_0$ [15].

In the present experiment two types of neon spectra have been recorded; firstly the integrated intensity of the optogalvanic signal as a function of laser wavelength and secondly the signal's temporal evolution following the optical excitation. The intent of recording the integrated optogalvanic spectra is to check the reliability and accuracy of our experimental set-up by verification of some previous work [16].

3.1 Time-resolved optogalvanic spectrum

The time-resolved optogalvanic spectrum was obtained at a fixed dye laser wavelength tuned in resonance with a dipole allowed electronic transition. The time-resolved signals were taken directly from the oscilloscope. In order to understand the collisional ionization of the excited states of neon atoms in gas discharge plasma, we selected three cases of neon transitions. A schematic energy level diagram and relevant transitions are shown in Figure 1. The solid lines in the figure represent the one-photon excitation that gives rise to the optogalvanic signal whereas dotted lines represent possible decay channels within the framework of the $j_c K$-coupling scheme. A theoretical model was developed by Han et al. [9], to characterize the dominant physical processes responsible for the optogalvanic signal in the discharge plasma. In this model it was assumed that the observed optogalvanic signal intensity as a function of time is the sum of the signals originating from all the energy states. The following expression was derived from the rate equation approach to extract the physics of

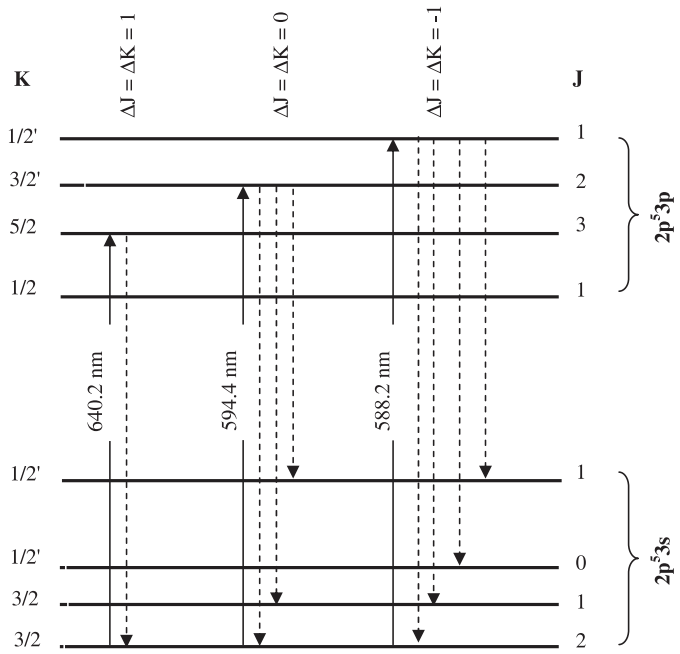

Fig. 1. Partial energy level diagram for neon transitions. The solid lines in the figure represent the one photon excitation that gives rise to the optogalvanic signal where as dotted lines represent the possible decay channels.

the time-resolved optogalvanic signal:

$$S(t) = \frac{a}{1-b\tau}\left[e^{-bt} - e^{-\frac{t}{\tau}}\right] + \frac{c}{1-d\tau}\left[e^{-dt} - e^{-\frac{t}{\tau}}\right]. \quad (1)$$

Here $S(t)$ is the signal intensity as a function of time, a and c are amplitudes, b and d are decay rates for the two levels involved in the transition and τ is the instrumental time constant of the waveform for the optogalvanic signal. The laser optogalvanic signal can be either positive or negative, composed of a fast rising peak followed by an exponential decay to the signal with an opposite sign, which then returns to the base line.

We have used a non-linear least square program to fit the observed time-resolved signals to the above equation and determined the amplitudes and decay rates of the aforementioned transitions. This expression reproduces the experimentally obtained time-resolved optogalvanic signal with only five parameters. In the following section we present the results for the three sets of transitions, which have been systematically investigated.

3.1.1 Case I ($\Delta J = \Delta K = -1$)

In this case, the experimentally observed time-resolved optogalvanic signal at wavelength 588.2 nm corresponding to the $2p^5 3s[3/2]_2 \rightarrow 2p^5 3p[1/2']_1$ transition has been selected to study the collisional ionization of the excited state in the neon discharge plasma. The observed time-resolved optogalvanic signal along with the fitted curve for a current of 3 mA is shown in Figure 2a. The waveform extends from 0 μs to 100 μs. By varying the discharge current from 1 mA to 5 mA, a set of time-resolved optogalvanic signals is compiled to reveal the effect of the discharge current. We have particularly selected this current range because if the current is less than the optimized value the temporal oscillations dominate the region where the optogalvanic signal normally appears. On the other hand if we increase the discharge current the signal saturates and no new information can be gathered from further increase in current. In Figure 2b the optogalvanic signals consist of fast rising peaks followed by decay to the negative side and then back to the base line level. Each spectrum shows a least square fit of the theoretical model (Eq. (1)) to the observed data of the time-resolved signal. At constant laser energy, the decay rates depend on the discharge current of the lamp i.e. higher current produces faster decay (see Tab. 1) and smaller peak intensities. With the increase of the discharge current the probability of ionization of the upper level $3p[1/2']_1$ increases. Because of the large ionization cross-section of the upper level an increase in its population results in higher ionization rates. This fact may be attributed to both an increase in the number density of atoms in the upper level and a change in the electron distribution function (see [10,17] and references therein). Thus the current will increase with the corresponding voltage decrease across the discharge to maintain the steady state condition. Consequently, the optogalvanic signal will decrease in magnitude. From Figures 2c and 2d it is noticed that there is a clear shift in the signal peaks as a function of the discharge current, which represents the positive and negative portions of the time-resolved signal (Fig. 2b). The change in the signal peak intensity as a function of discharge current was described in detailed in our previous work [10]. In Figure 2f changes in the signal amplitude as a function of discharge current are presented. It is evident from the plot that the variation of the signal amplitude as a function of current obeys an exponential law, consistent with the diffusive motion of electrons in the discharge plasma.

In the theoretical model [9] the decay rates are defined by

$$b = \Gamma_k + I\sigma_k \quad (2)$$

and

$$d = \Gamma_i + I\sigma_i. \quad (3)$$

Here b and d are the decay rates, σ_i and σ_k the electron collisional ionization rate parameters and Γ_k and Γ_i the effective decay rates of the upper and lower levels respectively. In the first column in Table 1 the discharge current is given while the other columns show the fitted parameters for the 588.2 nm transition. The decay rates ratio, amplitude ratio and the amplitude of the positive peaks are tabulated in the last two columns of this table.

The decay rates plots verses discharge current are shown in Figure 2e. It is noticed that within a certain discharge current range, the b and d values are linearly related to the discharge current. The observed data points are very well represented by the following parameters

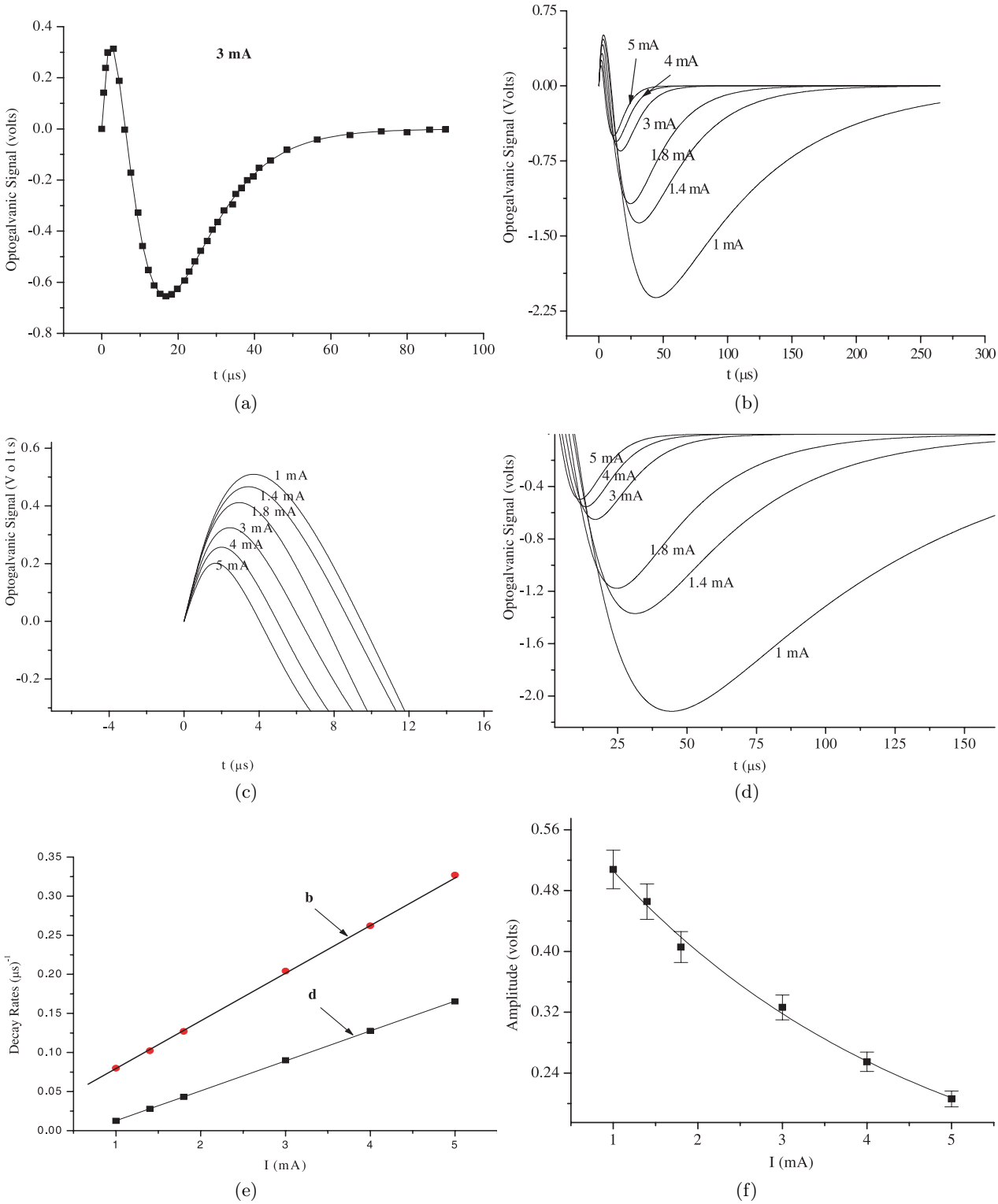

Fig. 2. Time-resolved optogalvanic signals of neon at 588.18 nm corresponding to $\Delta J = \Delta K = -1$ selection rules. (a) Solid line, which passes through the observed data points is the least square fit to equation (1). The signal was registered at 3 mA discharge current. (b) Set of time-resolved optogalvanic signals registered at different discharge currents. (c) The positive part of the optogalvanic signal reflects that as the hollow cathode current is increased the signal amplitude decreases and the peaks shift towards the shorter time scale. (d) The negative part of the optogalvanic signal shows that as the hollow cathode current is increased the signal amplitude approaches to the base line and the peaks shift towards the shorter time scale. (e) Plot of decay rates vs. discharge current. Solid lines are the least square fits to equations (2) and (3). (f) Plot of the optogalvanic signal amplitude vs. discharge current. The signal decreases with the increase of the discharge current.

Table 1. Data for time-resolved LOG signals of neon at 588.18 nm for different discharge currents.

I (mA)	Fitted parameters					Ratio		Amplitude (volts)±0.01
	a(V) ± 0.05	$b(\mu s)^{-1}$ ±0.005	c(V) ±0.05	$d(\mu s)^{-1}$ ±0.005	$\tau(\mu s)$ ±0.005	(b/d)	(a/c)	
1.0	5.88	0.079	–4.07	0.013	7.753	6.077	1.44	0.51
1.4	5.70	0.102	–3.90	0.028	6.406	3.643	1.47	0.47
1.8	6.03	0.127	–4.24	0.043	5.931	2.953	1.42	0.41
3.0	5.49	0.204	–3.78	0.090	5.051	2.266	1.45	0.33
4.0	5.64	0.262	–4.02	0.128	4.697	2.046	1.40	0.26
5.0	5.73	0.327	–4.16	0.165	4.618	1.982	1.38	0.20

obtained by linear regression fitting

$$b = 0.016 + 0.062\, I \tag{4}$$

$$d = -0.025 + 0.038\, I. \tag{5}$$

Here b and d are in $(\mu s)^{-1}$ and the discharge current I in mA. After comparing the theoretical decay rates (Eqs. (2, 3)) and observed decay rates (Eqs. (4, 5)), some important conclusions have been drawn.

(i) Lengthening of the effective life time of the upper level

The effective decay rate of the upper level $\Gamma_k = 0.016\ \mu s^{-1}$ reveals the effective lifetime of this state to be $\tau_k = 62.5\ \mu s$. This value is much larger than the radiative lifetime of the $3p[1/2']_1$ level, which is 18 ns [18]. Many other researchers ([8] and references therein, [19–21]) also reported the lengthening of the lifetime of the excited levels in the neon discharge plasma. The possible mechanism for this lengthening is attributed to radiation trapping. In the radiation trapping mechanism when atoms are excited by resonance radiation the resulting fluorescence from the volume occupied by the atoms may be delayed due to subsequent re-absorption and emission of the original fluorescent quanta. In the present case the upper level $2p^5 3p[1/2']_1$ is optically connected to the resonance levels $2p^5 3s[3/2]_1$ and $2p^5 3s[1/2']_1$ as well to the metastable levels $3s[3/2]_2$ and $3s[1/2']_0$. The radiation trapping occurs during the de-excitation of the aforementioned resonance levels in the discharge tube. This process is unique because the resonant radiation turns out to be trapped in the discharge tube. The emitted photon is absorbed by another atom so that the effective lifetime of the excitation within the system greatly exceeds the radiative lifetime of a level. Metastable population plays a key role in the ion production in many discharges. Its population is depleted through collisions and tube wall losses. Stewart et al. [8] calculated the tube wall losses, metastable densities, branching ratio and escape factor g. They used the expression for the escape factor given by Fujimoto et al. [22]

$$g = \frac{1 - k_0 r}{0.86 + k_0 r}.$$

Here $k_0 r$ is the optical thickness at the line center and r is the cylindrical radius. Due to limitations of our theoretical model and little information available about commercial hollow cathode we cannot relate imprisonment factor to our extracted values of the effective lifetimes. On the basis of previous work we may speculate that the lengthening of the effective lifetime of the upper level is due to radiation trapping.

(ii) Effective electron collisional ionization rate parameter

The extracted electron collisional ionization rate parameters for the upper and lower levels are $\sigma_k = 0.062\ \mathrm{mA}^{-1}\mu s^{-1}$ and $\sigma_i = 0.038\ \mathrm{mA}^{-1}\mu s^{-1}$ respectively. It is evident that the effective electron collisional ionization rate parameter of the upper level is larger than that of the lower level. The ratio of these two parameters (σ_k/σ_i) is 1.63, which is proportional to the total ionization cross-sections. However, the determination of the absolute magnitude of the cross-sections requires more experimental information. Since the upper level $2p^5 3p[1/2']_1$ has a larger ionization rate parameter therefore its population is increased because the ionization depends strongly on the population distribution of various levels [10]. On the basis of the ratio of the electron collisional ionization rate parameters (σ_k/σ_i) extracted in the present work, it is concluded that the electron collisional ionization is the dominant physical process contributing to the generation of the optogalvanic signal in the neon discharge plasma.

3.1.2 Case II ($\Delta J = \Delta K = +1$)

Secondly we studied the time-resolved optogalvanic signal associated with the transition $2p^5 3s[3/2]_2 \rightarrow 2p^5 3p[5/2]_3$ at 640.22 nm. In Figure 3a the solid line, which passes through the experimentally observed data points, is the result of the least squares fit with equation (1). A typical set of time-resolved optogalvanic signals extending from 0 μs to 50 μs at different currents is shown in Figure 3b. The set of time-resolved signals is compiled at constant laser energy. Each spectrum in the figure is a least square fit to the expression (1). From Figure 3b it is evident that the optogalvanic signals are composed of fast rising peaks followed by exponential decay of signal with opposite sign and then to converge back the base line. At higher current the signal intensity increases and obeys an exponential law (Fig. 3f). A possible explanation for this increase was given in our previous paper [10]. This change in the signal intensity indicates that the $2p^5 3p[5/2]_3$ upper level must be coupled with other $2p^5 3p$ configuration-based levels via collisions and its population may be partly transferred to some of the levels that are indirectly coupled to the ground level. The decay of these levels then results

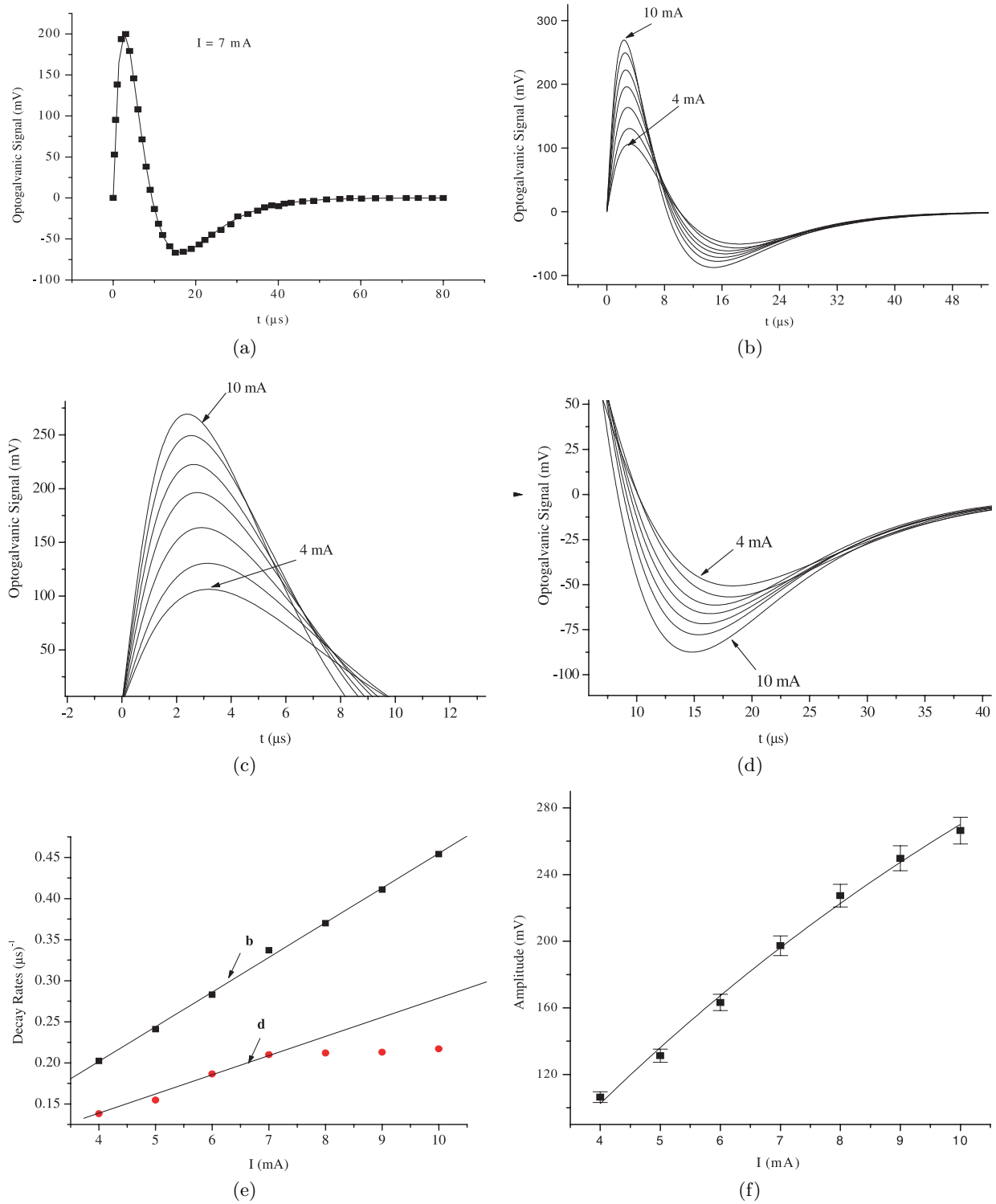

Fig. 3. Time-resolved optogalvanic signals of neon at 640.22 nm corresponding to $\Delta J = \Delta K = +1$ selection rules. (a) Solid line, which passes through the observed data points is the least square fit to equation (1). The signal was registered at 7 mA discharge current. (b) Set of time-resolved optogalvanic signals compiled at different discharge currents ranging from 4 mA to 10 mA. (c) The positive part of the optogalvanic signal reflects that as the hollow cathode current is increased the signal amplitude increases and the peaks shift towards the shorter time scale. (d) The negative part of the optogalvanic signal shows that as the hollow cathode current is increased the signal amplitude approaches to the base line and the peaks shift towards the shorter time scale. (e) Plot of decay rates vs. discharge current. The solid lines, which pass through the observed data points, are the least square fits to equations (2) and (3). (f) Plot of the signal amplitude vs. discharge current. The signal increases exponentially with the increase of the discharge current.

Table 2. Data for time-resolved LOG signals of neon at 640.22 nm for different discharge currents.

I (mA)	Fitted parameters					Ratio		Amplitude (mV)±0.01
	a(mV) ± 0.05	$b(\mu s)^{-1}$±0.005	c(mV)±0.05	$d(\mu s)^{-1}$±0.005	$\tau(\mu s)$±0.005	(b/d)	(a/c)	
4	1577.31	0.202	–1126.68	0.138	5.110	1.463	1.40	106.40
5	2038.25	0.241	–1353.66	0.154	6.159	1.557	1.51	131.21
6	3006.19	0.283	–2006.87	0.186	6.570	1.517	1.50	163.72
7	4100.26	0.337	–2574.09	0.211	7.815	1.605	1.59	197.26
8	4214.79	0.371	–2417.60	0.212	6.777	1.745	1.74	221.36
9	4414.32	0.411	–2321.08	0.213	6.908	1.929	1.90	249.78
10	4660.38	0.454	–2249.54	0.217	7.012	2.092	2.07	268.95

in a decreased metastable population, thus the current decreases and the voltage increases. The importance of collisions in the discharge plasma can be understood by comparing the collisional rates with the radiative rates. When the collisional rates dominate radiative rates, the excess population of the $2p^5 3p[5/2]_3$ level is transferred to the other $2p^5 3p$ configuration-based levels and consequently the atoms will quickly decay back to the $2p^5 3s$ configuration-based levels. The high collisional rates then quickly mix the population in the $2p^5 3s$ levels achieving a steady state value and the optogalvanic signal disappears. Since we have observed the optogalvanic signals on the microsecond time-scale, therefore the effective lifetime of the $2p^5 3p[5/2]_3$ must be of the order of microseconds. It is also apparent from Figures 3c and 3d that the signal peaks of both positive and negative parts of the time-resolved spectra are shifted with increasing the discharge current. The entire temporal profile of the signal shifts towards the shorter time scale. This shift in the signal peaks (both positive and negative) is attributed to the change of population and the effective lifetimes of the levels involved in the transition.

In this case the decay rates are also linearly related to the discharge current as has been observed in case I. The results of fitting b and d to equations (2, 3) over the range of the discharge current (4 mA to 10 mA) are plotted in Figure 3e. This figure clearly shows that the effective collision decay rate d-parameter follows a linear dependence up to 7 mA (discharge current), thereafter the data points show that as current increases the decay rate approaches saturation. The data points in the linear regression are represented by the following relations

$$b = 0.032 + 0.042\, I \tag{6}$$

$$d = 0.034 + 0.024\, I. \tag{7}$$

Comparing these equations with equations (2, 3), the effective decay rates of both the levels following the laser excitation are $\Gamma_k = 0.032\ \mu s^{-1}$ for the upper level and $\Gamma_i = 0.034\ \mu s^{-1}$ for the lower level. The effective lifetime for the upper level is 31.25 μs, which is much longer than the radiative lifetime, which is 19.4 ns [18]. The corresponding collisional ionization rate parameters are $\sigma_k = 0.042\ \mathrm{mA}^{-1}\,\mu s^{-1}$ and $\sigma_i = 0.024\ \mathrm{mA}^{-1}\,\mu s^{-1}$, respectively. The ratio of these two parameters (σ_k/σ_i) is calculated as 1.75, in good agreement with that reported by Han et al. [9]. It confirms that in this case again the electron collision ionization is the dominant physical process responsible for the production of the optogalvanic signal. In Table 2 the fitted parameters and the amplitudes at different discharge currents are presented. It is observed that the ratio of the decay rates and the ratio of the amplitude are almost identical.

3.1.3 Case III ($\Delta J = \Delta K = 0$)

In this case we concentrated specifically on the $2p^5 3s[3/2]_2 \rightarrow 2p^5 3p[3/2]_2$ neon transition at wavelength 594.48 nm, obeying $\Delta J = \Delta K = 0$ selection rules. Optogalvanic signal at different discharge currents were recorded. In Figure 4a a comparison between the fitted and the experimentally observed data is shown at 10 mA discharge current. A set of optogalvanic signals and an enlarged part of the positive and negative contributions are presented in Figures 4b–4d. Figure 4b shows that with increasing discharge current the signal intensity increases linearly. A possible explanation for this increase in the signal amplitude is attributed to a decrease in population of the metastable level. It is due to the coupling of the metastable level $2p^5 3p[3/2]_2$ with other $2p^5 3p$ configuration-based levels. Since these levels are indirectly coupled to the ground level therefore, the decay of these levels results in a decrease in the metastable population, thus a decrease in the current and an increase in the voltage occur. The decrease of the metastable concentration is linearly related to the discharge current (Fig. 4f) and consequently no shift in the signal peak positions occur.

The decay rates are also linearly related to the discharge current. From the plot of decay rates vs. discharge current (Fig. 4e) we conclude that the effective lifetime of the $2p^5 3p[3/2]_2$ level is 12.85 μs, which is longer than its radiative lifetime, 19 ns [18].

The extracted collisional rate parameters for the upper and lower levels are $\sigma_k = 0.011\ \mathrm{mA}^{-1}\mu s^{-1}$ and $\sigma_i = 0.011\ \mathrm{mA}^{-1}\mu s^{-1}$ respectively. The ratio of these parameters σ_k/σ_i is approximately equal to 1, which reveals that there are some other processes, other than the electron collisional ionization responsible for the optogalvanic signal. In Table 3 the fitted parameters, amplitudes, decay rates ratios and amplitudes ratios at different discharge currents are presented.

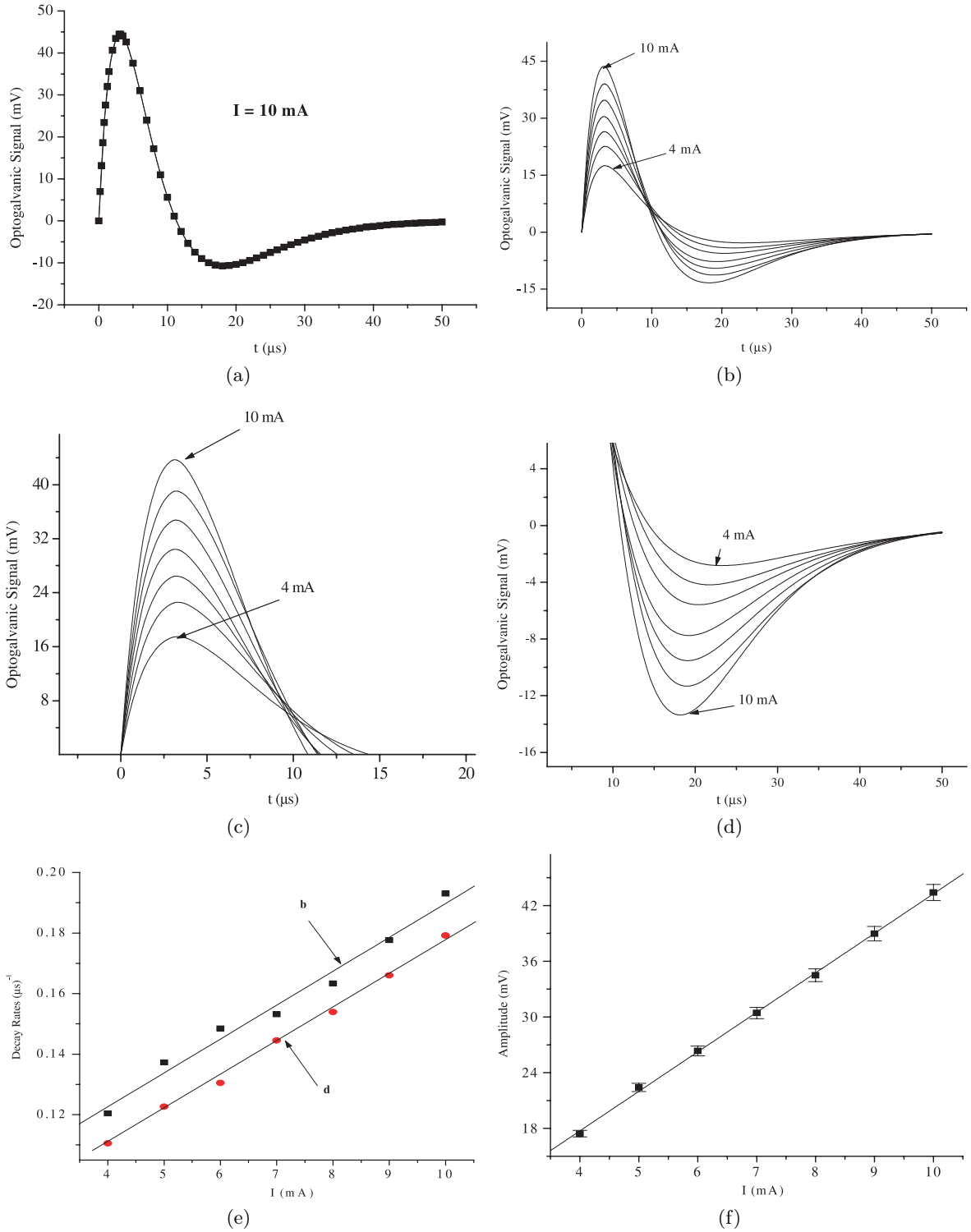

Fig. 4. Time-resolved optogalvanic signals of neon at 594.48 nm corresponding to $\Delta J = \Delta K = 0$ selection rules recorded at different discharge currents from 4 mA to 10 mA. (a) The solid line, which passes through the observed data points, is the least squares fit to equation (1). The signal was registered at a 10 mA discharge current. (b) Set of time-resolved optogalvanic signals compiled at different discharge currents. (c) The positive part of the optogalvanic signal demonstrates that as the hollow cathode current is increased the signal amplitude increases and the signal peaks remain at the same position. (d) The negative part of the optogalvanic signal reflects that as the hollow cathode current is increased the signal amplitude approaches to the base line and the peaks shift towards the shorter time scale. (e) Plot of decay rates vs. discharge current. The solid lines, which pass through the observed data points, are the least square fits to equations (2) and (3). (f) The plot of the signal amplitude vs. discharge current. The signal increases linearly with the increase of the discharge current.

Table 3. Data for time-resolved LOG signals of neon at 594.48 nm for different discharge currents.

I (mA)	Fitted parameters					Ratio		Amplitude (mV)±0.01
	a(mV) ± 0.05	$b(\mu s)^{-1}$±0.005	c(mV)±0.05	$d(\mu s)^{-1}$±0.005	$\tau(\mu s)$±0.005	(b/d)	(a/c)	
4	357.82	0.120	–320.97	0.111	2.604	1.081	1.11	17.43
5	418.34	0.137	–365.57	0.123	3.037	1.114	1.14	22.42
6	480.00	0.149	–412.50	0.131	3.150	1.137	1.16	26.34
7	1451.45	0.153	–1371.37	0.145	3.356	1.055	1.06	30.43
8	1750.05	0.163	–1641.51	0.154	3.868	1.058	1.07	34.50
9	2051.59	0.178	–1705.02	0.166	4.593	1.072	1.20	38.95
10	1964.67	0.193	–1792.06	0.179	4.802	1.078	1.09	43.40

Table 4. Results.

Wavelength (nm)	$\Delta J = \Delta K$ values	Collisional cross-section $(\text{mA})^{-1}(\mu s)^{-1}$		σ_k/σ_i	Effective lifetime τ_k (μs)	Maximum amplitude (mV)	Peak shifts (μs)	Change in amplitude with current
		σ_k	σ_i					
588.18	–1	0.062	0.038	1.63	62.5	507.80	2.088	decreases
594.48	0	0.011	0.011	1.00	12.85	43.40	0	increases
640.22	1	0.042	0.024	1.75	31.25	268.95	0.880	increases

4 Conclusion

In conclusion, we have been able to assess the dominant physical processes responsible for the optogalvanic signal on the basis of a detailed experimental study of the time-resolved optogalvanic spectra in the neon discharge plasma. It is noticed that the signal intensity dominates when ΔJ and ΔK change in the same direction i.e. $\Delta J = \Delta K = 0, \pm 1$. It is also noted that if the electron collisional ionization rate parameter σ_k of the upper level k is greater than electron collisional ionization rate parameter σ_i of the lower level i then the optogalvanic signal begins as a positive peak. On the other hand, if σ_k is less than σ_i, then the optogalvanic signal begins with a negative peak. However, if both σ_k and σ_i are comparable, the optogalvanic signal appears smaller in magnitude. We also have observed that the 640.22 nm transition depends strongly whereas the 588.18 nm transition depends less on the electron collisional ionization rate parameter while the 594.48 nm transition depends on other processes for the production of the optogalvanic signals.

The present work has been financial supported by the Pakistan Science Foundation project (120), Higher Education Commission (HEC), ICTP Trieste, Italy under the Affiliated Centre scheme, TWAS and the Quaid-i-Azam University, Islamabad

References

1. R.B. Green, R.A. Keller, G.G. Luther, P.K. Schenck, J.C. Travis, Appl. Phys. Lett. **29**, 727 (1976)
2. D.M. Pepper, IEEE J. Quant. Elect. **14**, 971 (1978)
3. G. Erez, S. Lavi, E. Miron, IEEE J. Quant. Elect. **15**, 1328 (1979)
4. J.E. Lawler, Phys. Rev. A **22**, 1025 (1980)
5. D.K. Daughty, J.E. Lawler, Phys. Rev. A **28**, 773 (1983)
6. E.M. van Veldhuizen, F.J. de Hoog, D.C. Schram, J. Appl. Phys. **56**, 2047 (1984)
7. E. de Marian, A. Sasso, J. Appl. Phys. **63**, 109 (1988)
8. R.S. Stewart, K.W. Mcknight, K.I. Hamad, J. Phys. D: Appl. Phys. **23**, 832 (1990)
9. X.L. Han, V. Wisehart, S.E. Conner, M.C. Su, D.L. Monts, Contrib. Plasma Phys. **34**, 439 (1995)
10. S. Mahmood, M. Anwar-ul-Haq, M. Riaz, M.A. Baig, Opt. Commun. **236**, 411 (2004)
11. G. Racah, Phys. Rev. **61**, 537 (1942)
12. R.D. Cowan, *The Theory of Atomic Structure and Spectra* (University of California Press, Berkeley, 1981)
13. N.E. Small-Warren, L.Y.C. Chiu, Phys. Rev. A **11**, 1777 (1975)
14. A. Sasso, M. Ciocca, E. Arimondo, J. Opt. Soc. Am. B **5**, 1484 (1988)
15. B.R. Reddy, P. Venkateswarlu, Opt. Commun. **85**, 491 (1991)
16. J.E.M. GoldSmith, J.E. Lawler Contemp. Phys. **22**, 235 (1981)
17. R. Shuker, A. Ben-Amer, G. Erez, Opt. Commun. **42**, 29 (1982)
18. A.A. Radzig, B.M. Smirnove, Ref. Data At. Mol. Ions 233 (1985)
19. R.S. Stewart, K.I. Hamad, K.W. McKnight, *Optogalvanic Spectroscopy* (Institute of Physics Conference Series, 1991), Vol. 113, p. 89
20. A.V. Phelps, Phys. Rev. **110**, 1362 (1958)
21. A.V. Phelps, Phys. Rev. **114**, 1011 (1959)
22. T. Fujimoto, C. Goto, K. Fukuda, Phys. Scr. **26**, 443 (1982)